CFD Modeling and Simulation of a lab-scale Fluidised Bed*

BRITT HALVORSEN and VIDAR MATHIESEN†

Keywords: *CFD, gas/particle flow, bubble formation, granular temperature*

The flow behaviour of a lab-scale fluidised bed with a central jet has been simulated. The study has been performed with an in-house computational fluid dynamics (CFD) model named FLOTRACS-MP-3D. The CFD model is based on a multi-fluid Eulerian description of the phases, where the kinetic theory for granular flow forms the basis for turbulence modelling of the solid phases. A two-dimensional Cartesian co-ordinate system is used to describe the geometry. This paper discusses whether bubble formation and bed height are influenced by coefficient of restitution, drag model and number of solid phases. Measurements of the same fluidised bed with a digital video camera are performed. Computational results are compared with the experimental results, and the discrepancies are discussed.

1. Introduction

Fluidised bed systems are of great interest in chemical process industry, pharmaceuticals production, mineral processing, energy related processes etc. Computational fluid dynamics (CFD) of multiphase flow processes provides a new tool for design and optimisation of multiphase flow systems such as fluidised reactors. CFD has during the last decades shown promising results and will probably become a useful tool in design of chemical reactors in near future (Mathiesen, 2000). However in order to be able to calculate complex industrial fluidised bed reactors, the bed expansion and bubble formation which dominate the flow have to be calculated correctly. This paper discuss the bubble formation and bed expansion for different kinds of drag models, magnitude of the coefficient of restitution and number of particle phases in a small-scale fluidised bed with a central jet.

2. Mathematical model

The simulation is performed using a CFD model (FLOTRACS-MP-3D), which is based on a multi-fluid Eulerian description of the phases. The kinetic theory for granular flow forms the basis for the turbulence modelling of the solid phases. A two-dimensional Cartesian co-ordinate system is used to describe the calculation domains.

Mathiesen *et al.* (2000*a*) and Mathiesen *et al.* (2000*b*) proposed a gas/solid flow model, which is generalized for one gas phase and N number of solid phases. This was done in order to describe particle size distributions more realistic. They gave a detailed description of the model, including a discussion of the consistency of the multiphase gas/particle model. This model is slightly modified here.

Each solid phase is characterized by a diameter, form factor, density and coefficient of restitution. The presence of each phase is described by a volume fraction varying from zero to unity. The laws of conservation of mass, momentum and granular temperature are satisfied for each phase individually. All the phases share a fluid pressure. The gas phase turbulence is modelled by a sub-grid scale (SGS) model (Deardorff, 1971). The largest scales are simulated directly, whereas the small scales are modelled with the SGS turbulence model. In order to calculate the fluctuations in the solid phases a conservation equation for granular temperature is solved for each solid phase.

2.1. *Governing equations*

2.1.1. *Continuity equations* The continuity equation for phase m is given by:

$$\frac{\partial}{\partial t}(\varepsilon_m \rho_m) + \frac{\partial}{\partial x_i}(\varepsilon_m \rho_m U_{i,m}) = 0 \tag{1}$$

where ε, ρ and U_i are the phase volume fractions, densities and the ith direction velocity components for phase m, respectively. No mass transfer is allowed between the phases.

2.1.2. *Momentum equations* The momentum equation in the j direction for phase m may be expressed as:

$$\frac{\partial}{\partial t}(\varepsilon_m \rho\, U_{j,m}) + \frac{\partial}{\partial x_j}(\varepsilon_m \rho_m U_{i,m} U_{j,m}) = -\varepsilon_m \frac{\partial p}{\partial x_j} + \frac{\partial \Pi_{ij,m}}{\partial x_i} + \varepsilon_m \rho_m g_j \tag{2}$$

$$+ \sum_{k=1, k \neq m}^{M} \Phi_{mk}(U_{j,k} - U_{j,m})$$

p is fluid pressure, g_j is j-direction component of gravity and Φ_{mk} is the drag coefficient between the phases m and k. The terms on the right side represent pressure forces, viscous forces, mass forces and drag forces respectively. Both gas-particle drag and particle-particle drag are included in the total drag.

Each phase is considered as an incompressible fluid. The stress tensor $\Pi_{ij,g}$ for the gas phase g is given by:

$$\Pi_{ij,g} = \mu_{eff,g}\left[\left(\frac{\partial U_j}{\partial x_i} + \frac{\partial U_i}{\partial x_j}\right) - \frac{2}{3}\delta_{ij}\frac{\partial U_k}{\partial x_k}\right]_g \tag{3}$$

where δ_{ij} is the Kroenecker delta. The effective viscosity is modelled by the SGS model proposed by Deardorff, (1971):

$$\mu_{eff,g} = \varepsilon_g \mu_{lam,g} + \varepsilon_g \rho_g (c_t \Delta)^2 \sqrt{S_{ij,g} : S_{ij,g}} \tag{4}$$

The turbulence model constant c_t is estimated to 0.079 by using the renormalization group (RNG) theory (Yakhot and Orszag, 1986).

$$S_{ij,g} = \frac{1}{2}\left[\frac{\partial U_j}{\partial x_i} + \frac{\partial U_i}{\partial x_j}\right]_g \tag{5}$$

$$\Delta = \sqrt[3]{\Delta x \Delta y \Delta z} \quad \text{in 3D and} \quad \Delta = \sqrt[2]{\Delta x \Delta y} \text{ in 2D}.$$

Δ is the characteristic length scale of the resolved eddies.

The total stress tensor $\Pi_{ij,s}$ for each solid phase s is:

$$\Pi_{ij,s} = -P_s\delta_{ij} + \mu_s\left(\frac{\partial U_j}{\partial x_i} + \frac{\partial U_j}{\partial x_i}\right)_s + \left(\xi_s - \frac{2}{3}\mu_s\right)\delta_{ij}\left(\frac{\partial U_k}{\partial x_k}\right)_s \tag{6}$$

The solid phase pressure P_s consist of a collision part and a kinetic part:

$$P_s = \sum_{n=1}^{N} P_{C,sn} + \varepsilon_s\rho_s\theta_s \tag{7}$$

$P_{C,sn}$ is the pressure caused by collisions between the solid phases s and n, and is expressed by:

$$P_{C,sn} = \frac{\pi}{3}(1+e_{sn})d_{sn}^3 g_{sn}n_s n_n \left\{\frac{m_0\theta_s\theta_n}{((m_s/m_n)\theta_s + (m_n/m_s)\theta_n)}\right\}\left\{\frac{(m_0/m_s)^2\theta_s\theta_n}{(\theta_s + (m_n/m_s)^2\theta_n)_n(\theta_s + \theta_n)}\right\}^{3/2} \tag{8}$$

$$e_{sn} = \frac{1}{2}(e_s + e_n) \quad \wedge \quad d_{sn} = \frac{1}{2}(d_s + d_n) \quad \wedge \quad m_0 = (m_s + m_n)$$

e, d, n, m and θ are coefficient of restitution, particle diameter, number of particles, mass of a particle and the granular temperature respectively. The coefficient of restitution is unity for fully elastic collisions and zero for inelastic collisions.

g_0 is the radial distribution function which is near one when the flow is dilute and becomes infinite when the flow is so dense that motion is impossible.

The radial distribution function is estimated by the model proposed by Ma and Ahmadi (1986):

$$g_0 = 1 + 4\varepsilon_s \frac{1 + 2.5000\varepsilon_s + 4.5904\varepsilon_s^2 + 4.515439\varepsilon_s^3}{\left[1 - \left(\dfrac{\varepsilon_s}{\varepsilon_{s,max}}\right)^3\right]^{0.67802}} \tag{9}$$

with $\varepsilon_{s,max} = 0.64356$.

When using more than one solid phase the binary radial distribution function is calculated by Mathiesen *et al.* (2000a):

$$g_{sn} = \frac{N}{2}\frac{g_0}{(1 - \varepsilon_g)}(\varepsilon_s + \varepsilon_n) \tag{10}$$

The solid phase bulk viscosity may be written as:

$$\xi_s \sum_{n=1}^{N} P_{C,sn}\frac{d_{sn}}{3}(\theta_s + (m_n/m_s)\theta_n)\sqrt{\frac{2}{\pi\theta_s\theta_n(\theta_s + (m_n/m_s)^2\theta_n)}} \tag{11}$$

The solid phase shear viscosity consists of a collision term:

$$\mu_{col,s} = \sum_{n=1}^{N} P_{C,sn}\frac{d_{sn}}{5}(\theta_s + (m_n/m_s)\theta_n)\sqrt{\frac{2}{\pi\theta_s\theta_n(\theta_s + (m_n/m_s)^2\theta_n)}} \tag{12}$$

and a kinetic term:

$$\mu_{kin,s} = \frac{2\mu_{dil,s}}{\dfrac{1}{N}\sum_{n=1}^{N}(1 + e_{sn})g_{sn}}\left\{1 + \frac{4}{5}\sum_{n=1}^{N}g_{sn}\varepsilon_n(1 + e_{sn})\right\}^2 \tag{13}$$

where:

$$\mu_{dil,s} = \frac{15}{8d_s^3} \varepsilon_s l_s \sqrt{\frac{2m_s \theta_{s,av}}{\pi}} \quad \wedge \quad l_s = \frac{1}{6\sqrt{2}} \frac{d_s}{\varepsilon_s} \tag{14}$$

To ensure that the dilute viscosity is finite as the volume fraction of solids approaches zero, the mean free path l_s is limited by the minimum control volume length.

The average granular temperature $\theta_{s,av}$ is proposed by Manger (1996):

$$\theta_{s,av} = \frac{2m_s \theta_s}{\left\{ \sum_{n=1}^{N} \left(\frac{n_n}{n_s}\right) \left(\frac{d_{sn}}{d_s}\right)^2 \sqrt{\frac{(m_0/m_s)^2 \theta_n}{(\theta_s + (m_n/m_s)^2 \theta_n)}} S^{3/2} \right\}^2} \tag{15}$$

$$S = \frac{(m_0/m_s)^2 \theta_n \theta_s}{(\theta_s + (m_n/m_s)^2 \theta_n)(\theta_n + \theta_s)}$$

A number of different gas-particle drag models have been proposed in the literature. Two of the most commonly used models are tested and discussed in this work. The total gas/particle drag coefficient may be expressed as:

$$\Phi_{sg} = \frac{3}{4} C_D \frac{\varepsilon_s \varepsilon_g}{d_s} \rho_g |\vec{U}_g - \vec{U}_s| \tag{16}$$

where C_D is friction coefficient and $\vec{U}$ is velocity vector. Gibilaro *et al.* (1985) proposed a model for the friction coefficient:

$$C_D = \frac{4}{3} \left(\frac{17.3}{Re} + 0.336 \right) \varepsilon_g^{-2.80} \tag{17}$$

where Re is the particle Reynolds number:

$$Re_s = \frac{d_s \rho_g |\vec{U}_g - \vec{U}_s| \varepsilon_g}{\mu_g} \tag{18}$$

The Erguns equation, Ergun (1952) in combination with the empirical model of Rowe (1961) is the second drag model applied in this work. This combination has been used in a number of studies e.g. Ding and Gidaspow (1990). The Ergun equation is based on the pressure drop per unit length over a fixed bed. This equation is assumed to be valid for dense flow conditions only. For $\varepsilon_g < 0.8$ the gas/solid drag coefficient is expressed by:

$$\Phi_{sg} = 150 \frac{(1-\varepsilon_g)^2 \mu_g}{\varepsilon_g d_s^2} + 1.75 \frac{\rho_g |\vec{U}_g - \vec{U}_s| \varepsilon_s}{d_s}, \quad \text{for } \varepsilon_g \leqslant 0.8 \tag{19}$$

For void fractions $\varepsilon_g > 0.8$ the drag coefficients are based on the work by Rowe (1961) and Wen and Yu (1966):

$$\Phi_{sg} = \frac{3}{4} C_D \frac{\rho_g \varepsilon_s \varepsilon_g}{d_s} |\vec{U}_g - \vec{U}_s| \varepsilon_g^{-2.65}, \quad \text{for } \varepsilon_g > 0.8 \tag{20}$$

The friction coefficient is related to Reynolds number by:

$$C_D = \frac{24}{Re_s}(1 + 0.15 Re^{0.687}), \qquad Re_s \leqslant 1000 \tag{21}$$

$$C_D = 0.44, \qquad Re_s > 1000$$

The Reynolds number is as defined in (18).

The particle/particle drag coefficient is proportional to the particle collision pressure as given by Manger (1996):

$$\Theta_{sn} = P_{C,sn} \left\{ \frac{3}{d_{sn}} \sqrt{\frac{2(m_s^2 \theta_s + m_n^2 \theta_n)}{\pi m_0^2 \theta_s \theta_n}} \right.$$

$$\left. + \frac{1}{|\vec{u}_n - \vec{u}_s|} \left[\nabla \left| \ln \frac{\varepsilon_s}{\varepsilon_n} \right| + \frac{\theta_s \theta_n}{\theta_s + \theta_n} \left| \frac{\nabla \theta_n}{\theta_n^2} - \frac{\nabla \theta_s}{\theta_s^2} \right| + 3\nabla \left| \frac{\ln(m_n \theta_n)}{\ln(m_s \theta_s)} \right| \right] \right\} \tag{22}$$

2.1.3. Granular temperature equations In recent continuum models (e.g. Gidaspow (1994), Mathiesen *et al.* (2000a), Goldscmidt *et al.* (2001)) equations according to the kinetic theory of granular flow are incorporated. This theory describes the dependence of the rheologic properties of the fluidised particles on local particle concentration and the random fluctuating motion of particles due to particle-particle collisions. The granular temperature for a particle is defined as:

$$\theta = \frac{1}{3} \langle C \cdot C \rangle \tag{23}$$

where C is the fluctuating component of the particle velocity. The variation of particle velocity fluctuation is described with a separate conservation equation, the granular temperature equation. The transport equation for granular temperature is solved for each solid phase, and is given by:

$$\frac{3}{2} \left[\frac{\partial}{\partial t} (\varepsilon_s \rho_s \theta_s) + \frac{\partial}{\partial x_i} (\varepsilon_s \rho_s U_{i,s} \theta_s) \right] = \left(\Pi_{ij,s} : \frac{\partial U_{j,s}}{\partial x_i} \right) + \frac{\partial}{\partial x_i} \left(\kappa_s \frac{\partial \theta_s}{\partial x_i} \right) - \gamma_s - 3\Phi_{sg} \theta_s \tag{24}$$

The conductivity of granular temperature κ_s and the dissipation due to inelastic collisions γ_s, are determined from the kinetic theory for granular flow. The conductivity is given by a collision and a kinetic part as:

$$\kappa_s = \frac{2\kappa_{dil,s}}{\frac{1}{N} \sum_{n=1}^{N} (1 + e_{sn}) g_{sn}} \left\{ 1 + \frac{6}{5} \sum_{n=1}^{N} g_{sn} \varepsilon_n (1 + e_{sn}) \right\}^2 + 2\varepsilon_s \rho_s d_s \sqrt{\frac{\theta_s}{\pi}} \sum_{n=1}^{N} \varepsilon_n g_{sn}(1 - e_{sn}) \tag{25}$$

where:

$$\kappa_{dil,s} = \frac{225}{32} \varepsilon_s l_s \sqrt{\frac{2m_s \theta_{s,av}}{\pi}} \tag{26}$$

The first term on the right side of equation (25) dominates in dilute flow whereas the second term dominates in dense flow.

The dissipation of turbulent kinetic energy due to inelastic collisions γ_s is given by:

$$\gamma_s = \sum_{n=1}^{N} \frac{3}{4} P_{C,sn} \frac{(1-e_{sn})}{d_{sn}} \left[4\sqrt{\frac{2\theta_s\theta_n}{\pi((m_s/m_0)^2\theta_s + (m_n/m_0)^2\theta_n)}} \right.$$

$$\left. - d_{sn}\left(\frac{(m_s/m_0)\theta_s + (m_n/m_0)\theta_n}{(m_s/m_0)^2\theta_s + (m_n/m_0)^2\theta_n}\right) \right] \frac{\partial U_{k,s}}{\partial x_k} \qquad (27)$$

2.2. *Numerical solution procedure*

The governing equations are solved by a finite volume method, where the calculation domain is divided into a finite number of non-overlapping control volumes. Volume fraction, density and granular temperature are stored at main grid points placed in centre of the control volumes. Staggered grid arrangements are used for the velocity components that are stored at the main control volume surfaces. The conservation equations are integrated in space and time. This integration is performed using first order upwind differencing in space and fully implicit in time. The set of algebraic equations is solved by a tri-diagonal matrix algorithm (TDMA), except for the volume fraction where a point iteration method is used. Due to the strong coupling between the phases through the drag forces, the two-phase partial elimination algorithm (PEA) is generalized to multiple phases and used to decouple the drag forces. The interphase-slip algorithm (IPSA) is used to take care of the coupling between the continuity and the velocity equations.

3. Experimental and computational set-up

3.1. *Experimental set-up*

A two-dimensional bed is constructed in order to study the bed expansion and bubble formation in gas/solid flow. The purpose of this experimental study is to verify the predictive capability of the CFD model. The fluidised bed is constructed with a cross-sectional area of 19.5×2.5 cm and a height of 63 cm. The central jet is a 0.5×2.5 cm rectangular slit. The pressure drop through the distribution section is about 15% of the bed weight. The experimental set-up is shown in Figure 1, and the experimental conditions are given in Table 1.

Spherical glass particles with a particle density of 2485 kg/m^3 and a settled bulk density of 1500 kg/m^3 are applied in the experiments. The volume average mean particle diameter is measured to be 550 μm. The void fraction in the settled bed is estimated to 0.396.

The initial bed height of the fluidised bed is 28 cm. The bed is fluidised by introducing compressed air with a velocity of 0.29 m/s through the air distributor. Jet air is injected at a velocity of 4.9 m/s. A digital video camera is applied to measure bubble formation and velocity.

3.2. *Computational set-up*

A two-dimensional Cartesian co-ordinate system is used to describe the geometry. The grid is uniform in both horizontal and vertical direction. 39 and 63 control volumes are used in the horizontal and vertical direction respectively. Computational set-up is given in Table 2.
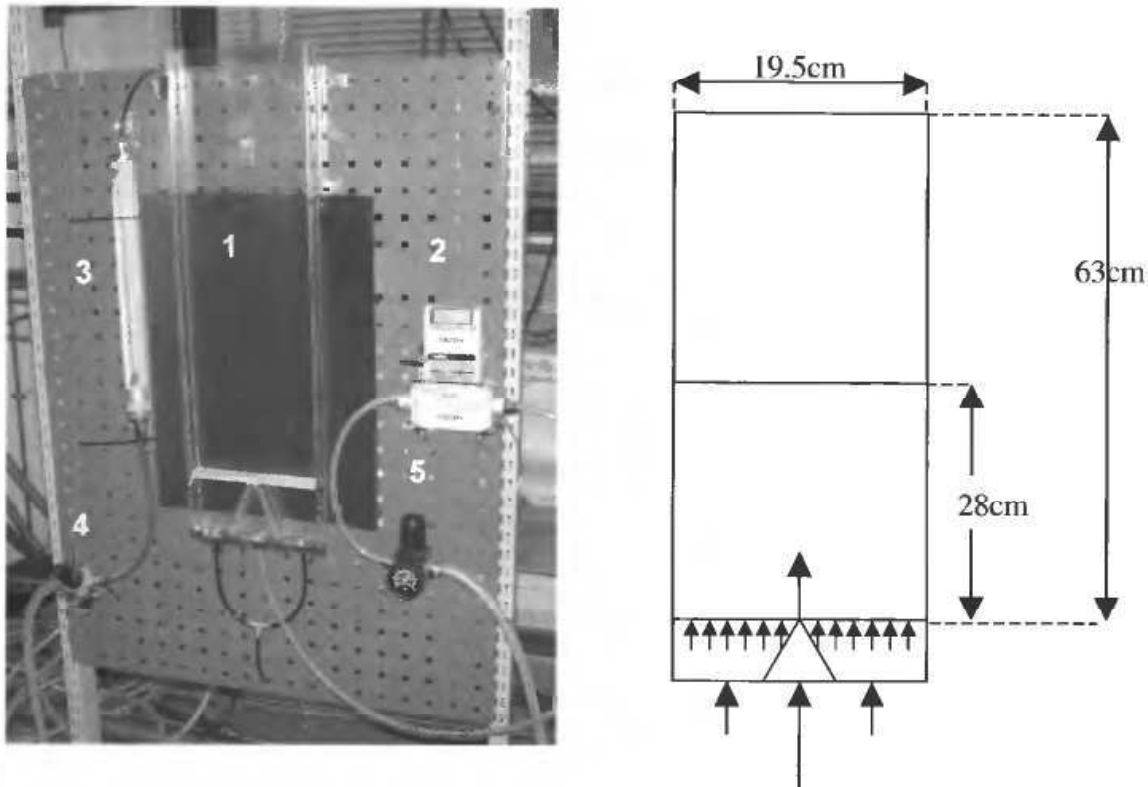
Figure 1. Experimental set-up.

Table 1. Experimental conditions

Height	63.0 cm	Initial bed height	28.0 cm
Width	19.5 cm	Fluidisation velocity	0.29 m/s
Depth	2.50 cm	Jet velocity	4.9 m/s
Mean particle size	550 μm	Solid density	2 485 kg/m³
Freeboard pressure	101 325.0 Pa	Bulk density	1 500 kg/m³

Table 2. Computational set-up

Height	63.0 cm	Horizontal grid size	5.0 mm
Width	19.5 cm	Vertical grid size	10.0 mm
Initial bed height	28.0 cm	Gas phase shear viscosity	$1.8 \cdot 10^{-5}$ Pa s
		Initial void fraction	0.50
One phase		Maximum volume fraction of solids	0.64356
Particle mean diameter	550 μm	Jet velocity	4.9 m/s
Three phases		Fluidisation velocity	0.29 m/s
Particle mean diameter	630 μm (18%)	Freeboard pressure	101 325.0 Pa
	500 μm (50%)	Solid density	2 485 kg/m³
	400 μm (32%)	Bulk density	1 500 kg/m³

Simulations have been run with both one and three solid phases in order to discuss possible improvement of several solid phases.

4.   Experimental and computational results

The experimental results are presented in section 4.1. In section 4.2 the simulations with one and three particle phases are compared with each other. The drag models influence on bubble formation and expanded bed height is studied by using two different drag models, Ergun/Wen and Yu drag model is compared against the drag model by Gibilaro *et al.* (1985). The numerical results of this are presented in section 4.3.

In order to study the influence of the coefficient of restitution on the bubble formation, simulations with four different values are performed. These results are given in section 4.4. The experimental and computational results are compared with each other in section 4.5.

A bubble is assumed to be a region of void fraction greater than 0.80. Gidaspow (1994) used this definition of a bubble. Kuipers *et al.* (1991) defined the bubble contour as a void fraction of 0.85.

4.1. *Experimental results*

A movie sequence of the experimental results is shown in Figure 2. Between 0 and 0.120 s the bubble size increases, but is located at the approximate same vertical position. At time 0.120 s the bubble diameter is 4.2 cm, and the bubble starts to rise. The bubble is circular, and the diameter increase to 6.5 cm during the next 0.200 s. Between 0.320 s and 0.740 s the bubble moves from bed height 12 cm to 28 cm. During this rise, the shape of the bubble changes and bubble break-up is observed. The vertical diameter decreases from 6.5 cm to about 2 cm and the horizontal diameter increases from 6.5 to 8.5 cm. After 0.800 s the first bubble has erupted.

A new bubble is formed and starts to rise after 0.440 s. This bubble moves faster and differs significantly in shape from the first one. At time 0.740 s the lower part of the bubble has reached a height of 14 cm. The horizontal diameter is 3.6 cm and the vertical diameter is 5.5 cm. The first bubble in the same position was splitted, and had a horizontal and vertical diameter of 6.7 cm and 3.6 cm respectively. The bed height is observed in the centre of the column, and increases from 28 cm at time 0, to 32 cm at 0.800 s.

4.2. *Simulations with one and three particle phases*

In the multi-fluid Eulerian model the particle mixture can be divided into a discrete number of phases, whereby different physical properties can be specified for each particle class. In this study three particle phases have been included in the simulations. Each of these phases has its own particle size, whereas the particle density and the coefficient of restitution remain constant. A corresponding case with one particle phase has been simulated, and the numerical results have been compared. Figures 3 and 4 show the results from the simulations with one and three particle phases respectively. Erguns drag model is used in these simulations and the coefficient of restitution is 0.99.
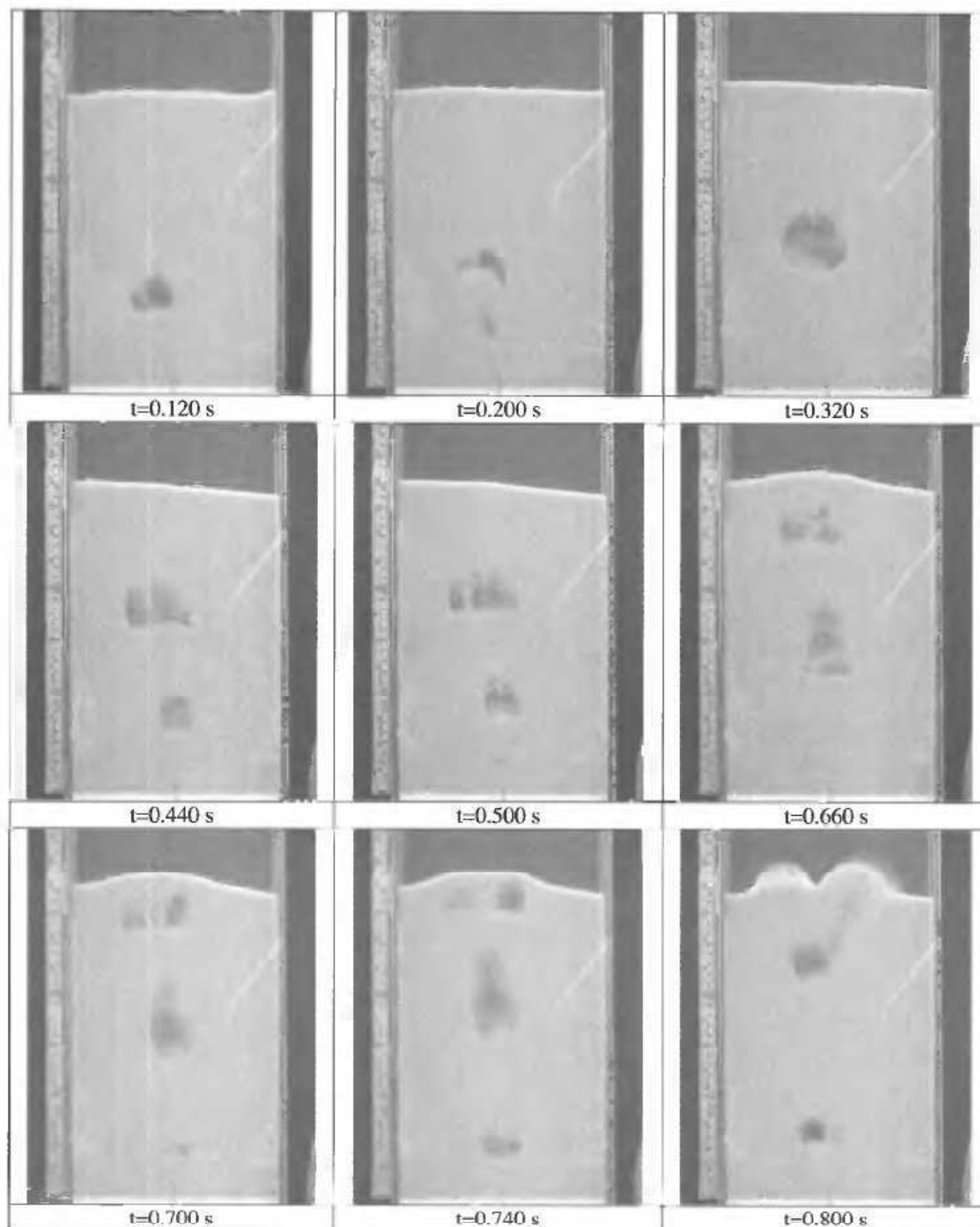
Figure 2. A movie sequence of experimental results.

Comparisons of the simulations with one and three particle phases show that one particle phase gives a smaller bubble. It seems that the vertical diameter becomes smaller, and that the bubble get a more spherical shape for one than for three solid phases. The simulation with one particle phase does not produce any further bubbles after the first bubble has erupted.

Figure 4 shows that the simulation with three particle phases gives a continuous bubble formation. The first bubble differs significantly from the next in shape, size and velocity. The second, third etc bubbles seem to break-up near the top of the bed.
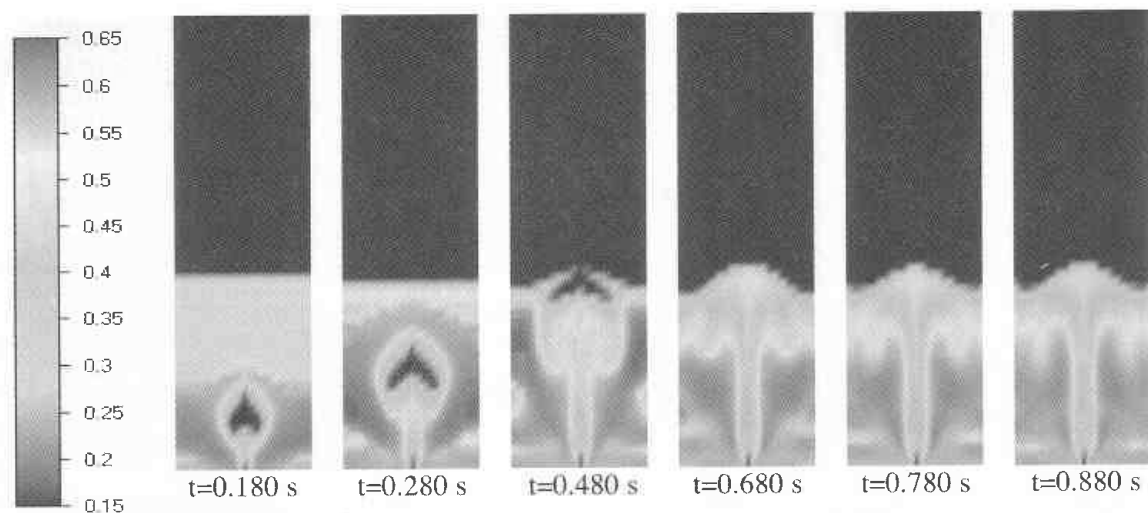
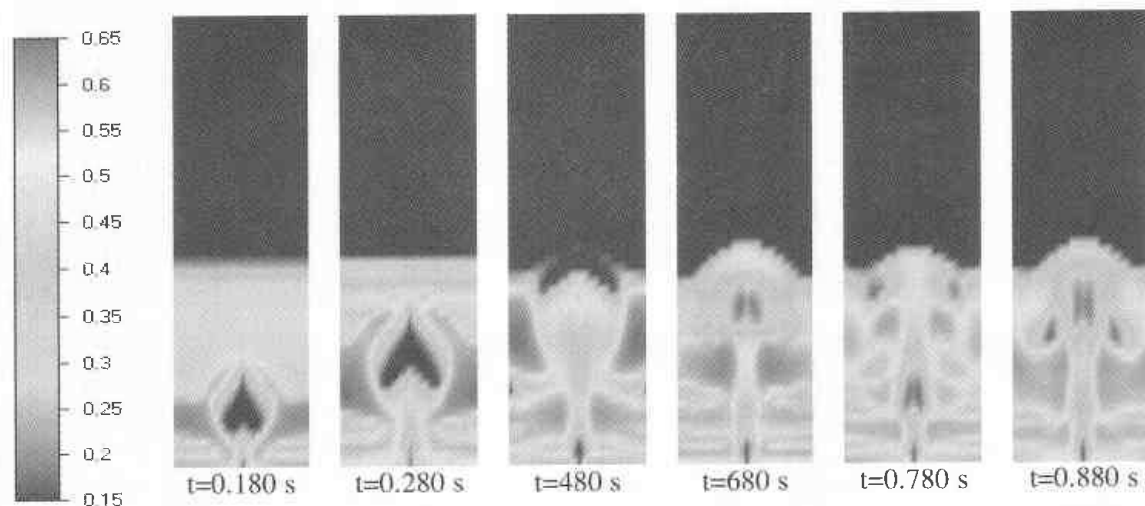Figure 3.   Volume fraction of solids, simulation with one particle phase.

Figure 4.   Volume fraction of solids, simulation with three particle phases.

The bed height in the centre of the bed is estimated for the two cases. The bed height increased from initial 28 cm to 29.2 cm in the case with one particle phase, and from 28 cm to 33 cm in the case with three particle phases. After the first bubble has erupted, the bed height is almost constant for both cases. Since the simulation with three solid phases gives a continuous bubble formation, whereas the single solid phase does not, the next simulations are performed with three solid phases.

4.3. *Results from simulations with different drag models*

Figures 5 and 6 show the results from the simulations with Ergun/Wen and Yu drag model and Gibilaro *et al.* (1985) drag model respectively. Three particle phases are included in the simulations. Particle diameter and initial volume fraction of each phase are given in Table 2. The coefficient of restitution is 0.99 for all phases.

Figures 5 and 6 it shows that the simulations with Erguns drag model differ considerably from the simulations with Gibilaro *et al.* (1985) drag model. The
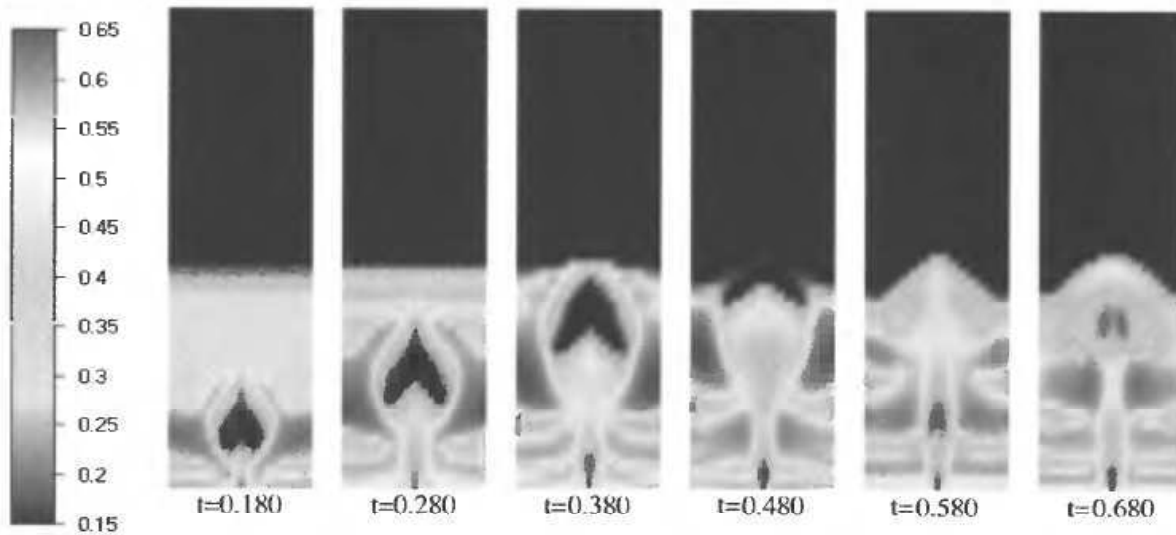
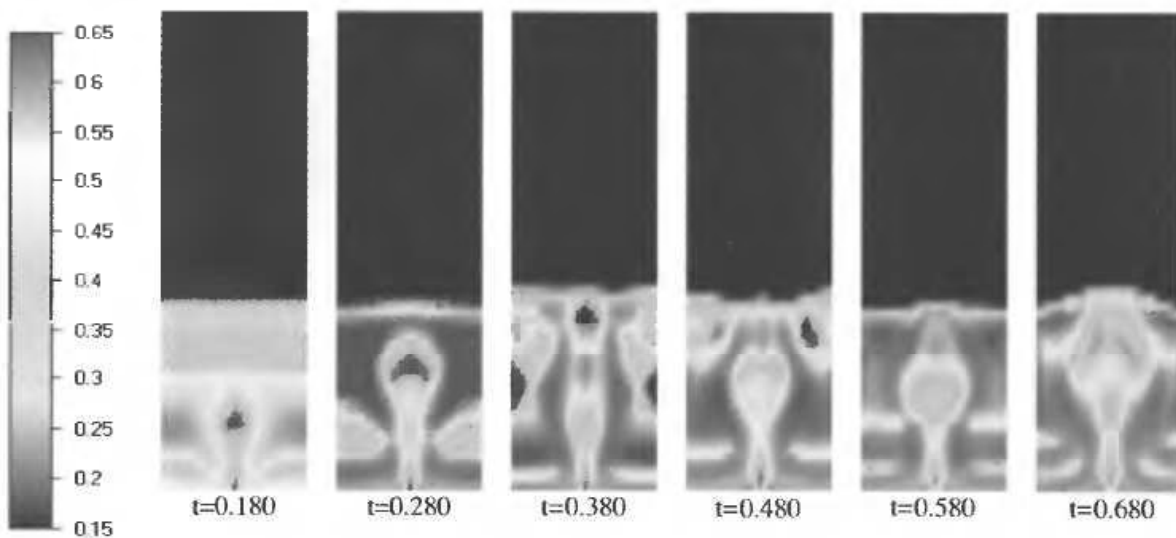Figure 5.   Volume fractions of solids, simulation results by using Erguns drag model.

Figure 6.   Volume fractions of solids, simulation results by using Gibilaros drag model.

simulation with Erguns drag model gives a heart shaped bubble that increases in size during the rise through the bed. The first bubble that is formed differs significantly from the next bubbles both in shape and size. Gidaspow (1994) did the same observation in his experiments and simulations. New bubbles are formed continuously. All the bubbles are created and rise in the centre of the model.

The bed height expands from initial 28 cm to 33 cm. After eruption of the first bubble, the height is nearly constant. The velocity of the first bubble is estimated to 0.56 m/s. The next bubbles move faster.

Figure 6 shows that simulation with Gibilaros drag model gives bubble formations both in the centre and close to the walls. After eruption of the first bubble there is no further bubble formation in the centre that satisfies the definition of a bubble. The simulation gives high concentrations of particles in most part of the bed, and the volume fraction exceeds the maximum specified volume fraction in some regions. The bed height varies between 28 cm and 25.6 cm during the run.

A comparison of the two drag models shows that Erguns model gives the largest bubbles, the highest bed and the lowest concentration of particles. The measurements presented in section 4.1 confirm that the Ergun model calculates a more reasonable bubble formation and bed height for this flow condition.

4.4. *Results from simulations with different coefficients of restitution*

The effect of varying the coefficient of restitution is studied with three particle phases. Ergun/Wen and Yu drag model is used in the simulations, further simulation conditions are given in Table 2.

Figures 7, 8 and 9 shows the results from the simulations with various coefficients of restitution at time 0.180 s, 0.380 s and 0.580 s, respectively. The numerical results indicate that the bubble velocity and the shape of the first bubble seem to be almost independent of the coefficient of restitution. However, it seems that the coefficient of restitution influences the bubble size and local concentration of solids. Decreasing coefficient of restitution gives an increasing bubble diameter. The maximum concentration of solids increases significantly when the coefficient of restitution is decreased from 1 to 0.95.

After 0.580 s (Figure 9) the first bubble has erupted, and by using unity coefficient of restitution, no further bubbles are formed. Lower values for e gives continuous bubble formations. Simulations with $e = 0.99$ seems to give the most realistic results, whereas simulations with lower coefficient of restitution give an unrealistic high local volume fraction of solids.

4.5. *Comparison between computational and experimental results*

Figures 10, 11 and 12 show a comparison between computational and experimental bubbles at three levels in the bed. The computational bubbles are simulated
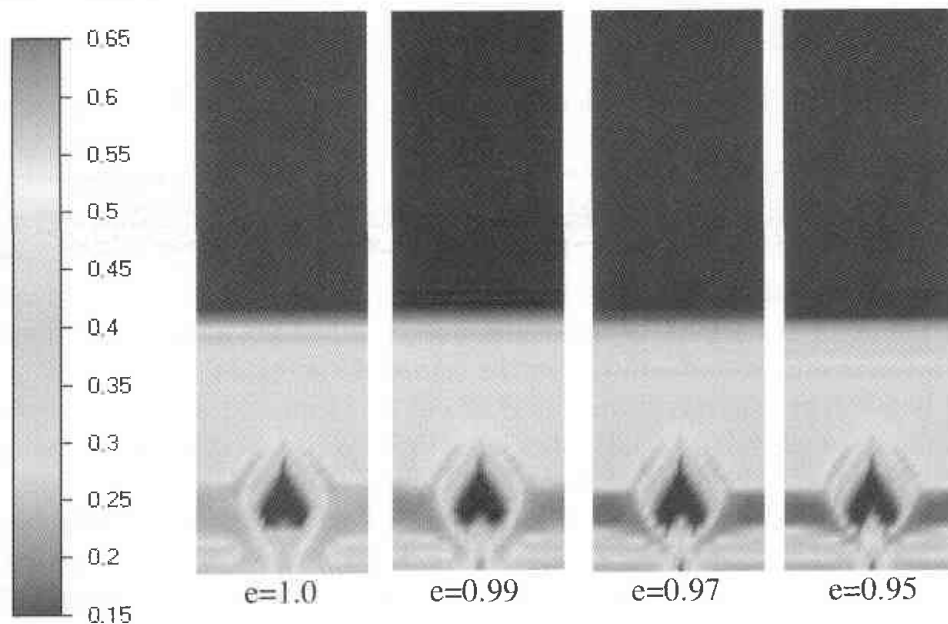

Figure 7.   Volume fraction of solids, simulations with various values of the coefficient of restitution at time t = 0.180 s.
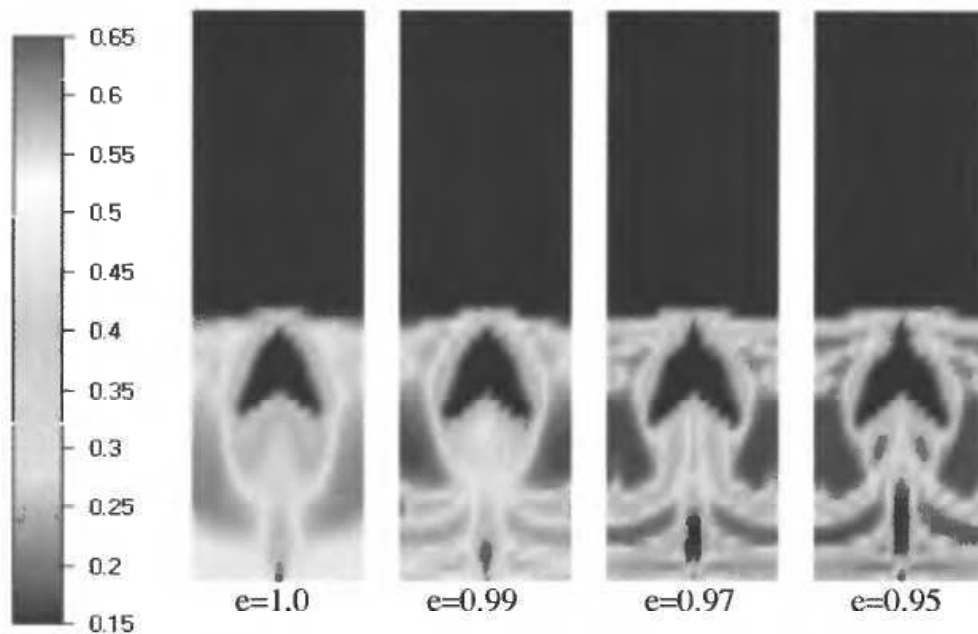
Figure 8.   Volume fraction of solids, simulations with various values of the coefficient of restitution at time t = 0.380 s.
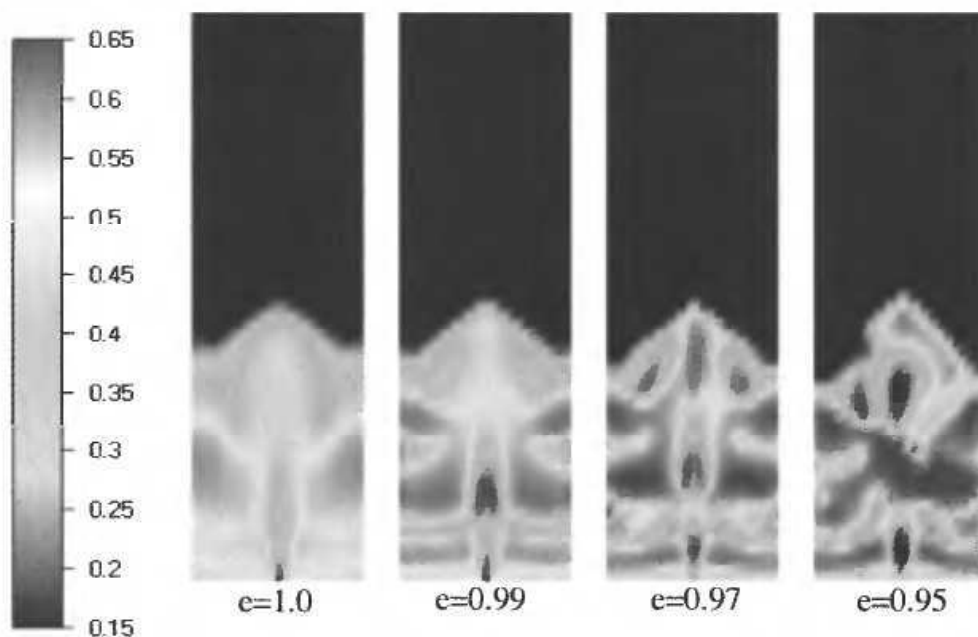

Figure 9.   Volume fraction of solids, simulations with various values of the coefficient of restitution at time t = 0.580 s.

with three particle phases, Erguns drag model and the coefficient of restitution like 0.99.

Figure 10 shows the bubbles 12 cm above the air inlet. There is observed discrepancies in shape between the experimental and computational bubble, although horizontal diameter of the bubbles is almost the same, approximately 6.5 cm.

The numerical result shows a bubble with an unphysical pointed shape. This is probably due to numerical diffusing resulting from the use of first order upwind scheme. A second order scheme will probably avoid this unphysical behavior.
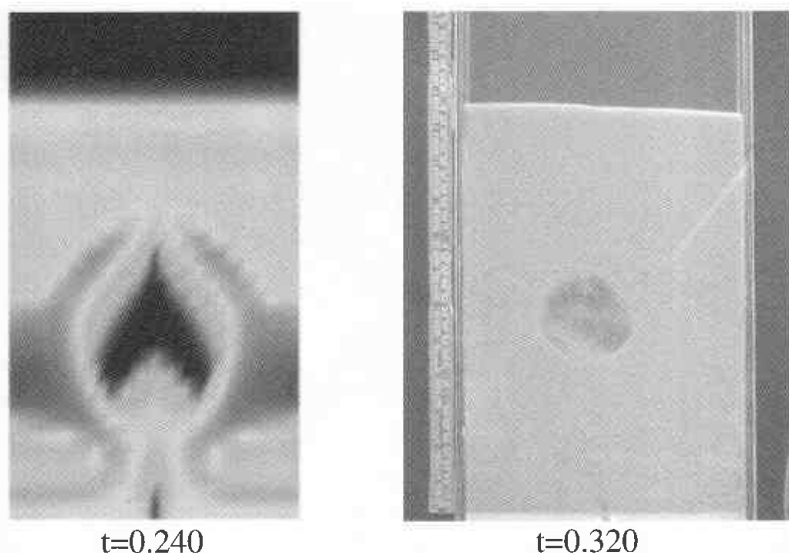
t=0.240   t=0.320

Figure 10.   Computational vs. experimental bubble at bed height 12 cm.

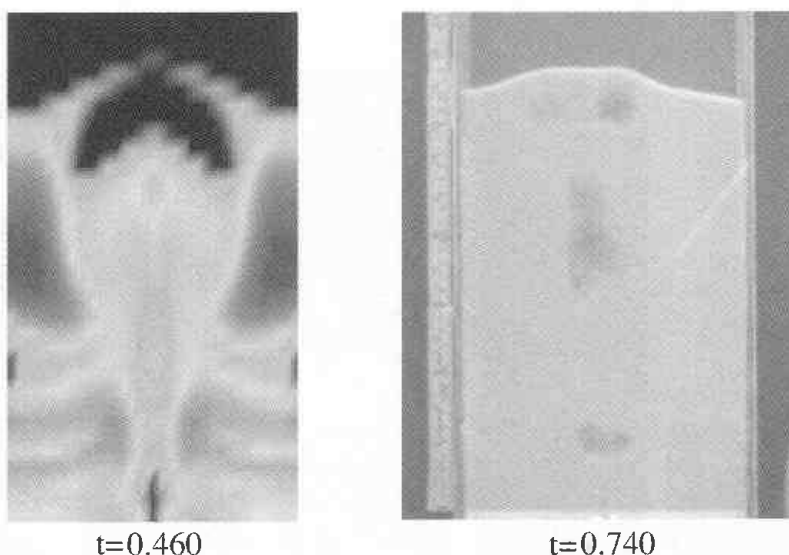t=0.460   t=0.740

Figure 11.   Computational vs. experimental bubble near the top of the bed.

At the next level, shown in Figure 11, both the computational and the experimental bubble have changed. The horizontal diameters have increased and the vertical diameters have decreased. In both directions the computed bubble is somewhat larger than the bubble from the experiment.

The numerical bubble velocity is significantly higher than the experimental. This can be observed from the difference in time at comparable levels. The bed height measured in centre of column is almost identical. This may be explained by the initial volume fraction, which is 0.5 in the simulations.

Figure 12 shows a comparison of the computational and experimental second bubble. These bubbles seem to have closely the same shape, but the experimental bubble is larger than the computed bubble.
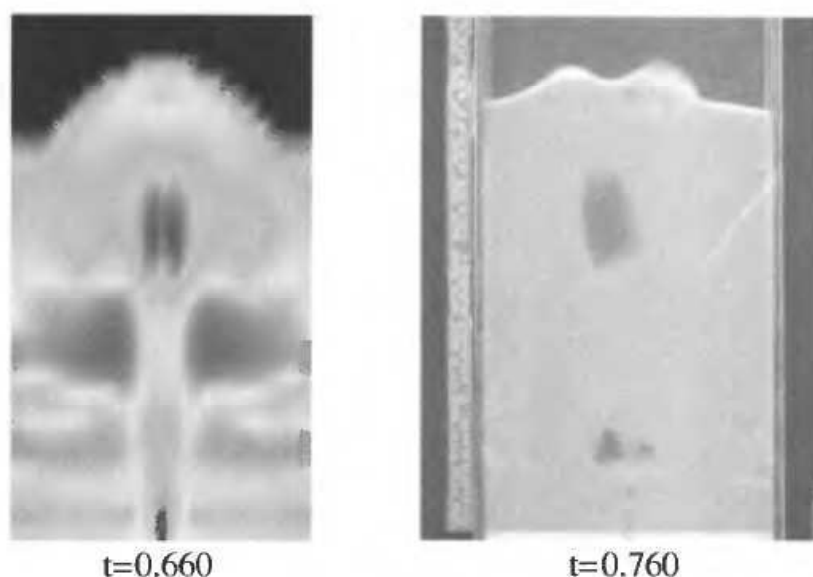
t=0.660   t=0.760

Figure 12.   Computed vs. experimental bubble. The second bubble is considered at the bed height 20 cm.

5.   Conclusion

Two-dimensional simulations of a lab scale fluidised bed with a central jet are performed. The simulations are performed with different drag models, various values for the coefficients of restitution and with one and three particle phases. The computational results with different simulations conditions have been compared.

It is shown that Erguns drag model and Gibilaro *et al.* drag model gives significant different bubble formation and bed height. One reason can be that Gibilaro *et al.* cover the whole range of flow conditions, both dilute and dense flow, whereas Ergun is valid under dense flow conditions.

The coefficient of restitution has an effect on the bubble size, the concentration of particles and the bubble formation. Simulations with more than one particle phase are performed. The comparison between simulations with one and three solid phases shows that three solid phases give continuously bubble formations whereas one solid phase give formation, rise and eruption of only the first bubble. Simulations with one particle phase give a smaller bubble.

A selection of the computational results has been compared with experimental results. The simulations give a higher bubble velocity and a larger bubble than the experiments. The difference in velocity may partly be due to the initial volume fraction that is used in the simulations. Higher initial volume fraction of solids will result in a lower bubble velocity, but also a larger bubble.

The shape of the bubbles also differs significantly, probably due to numerical diffusion resulting from the use of first order upwind scheme. A second order scheme reduces the numerical diffusion significantly, and may calculate more realistic bubbles.

Notation

C_d	drag coefficient
c_t	constant in Sub Grid Scale model
d	particle diameter
d_{sn}	mean particle diameter $= 0.5(d_s + d_n)$

e	coefficient of restitution
e_{sn}	mean coefficient of restitution $= 0.5(e_s + e_n)$
g_i	i-direction component of gravity
g_0	radial distribution function for a single solid phase
g_{sn}	binary radial distribution function
l	mean free path
M	number of phases
m	mass of a particle
m_0	binary mass $= m_s + m_n$
N	number of solid phases
n	number of particles
p	fluid pressure
P_C	collisional pressure
P_s	solid phase pressure
Re_s	particle Reynolds number
U_i, U_j	i and j components of velocity

Greek symbols

ε	volume fraction
$\varepsilon_{s,max}$	maximum volume fraction of solids
β_i	area porosity in i direction
β_V	volume porosity
γ	collisional energy dissipation
δ_{ij}	Kroenecker delta
θ	granular temperature $= 1/3 \langle C_s^2 \rangle$
κ	transport coefficient of granular temperature
μ	shear viscosity
ξ	bulk viscosity
Π_{ij}	stress tensor, solid phase
ρ	density
Φ	drag coefficient

Subscripts

av	average
col	collisional
dil	dilute
eff	effective
g	gas phase
kin	kinetic
lam	laminar
m	gas phase or solid phase m
n	solid phase n
s	solid phase s

References

DEARDORFF, J. W. (1971). On the Magnitude of Subgrid Scale Eddy Coefficient. *Journal of Computational Physics*, **7**, 120–133.

DING, J. and GIDASPOW, D. (1990). Bubbling fluidization model using kinetic theory of granular flow. *AIChE Journal*, **36**(4), 523–538.

GIDASPOW, D. (1994). Multiphase Flow and Fluidization. Academic Press, Boston.

GOLDSCHMIDT, M. J. V., KUIPERS, J. A. M. and VAN SWAAIJ, W. P. M. (2001). Hydrodynamic modelling of dense gas-fluidised beds using the kinetic theory of granular flow: effect of coefficient of restitution on bed dynamics. *Chemical Engineering Science*, **56**, 571–578.

KUIPERS, J. A. M., VAN DUIN, K. J., VAN BECKUM, F. P. H. and VAN SWAAIJ, W. P. M. (1991). A numerical model of gas fluidized beds. Chemical Engineering Science, **47**(8), 1913–1924, 1992.

MA, D. and AHMADI, G. (1986). An equation of state for dense rigid sphere gases, *Journal of Chemical Physics*, **84**(6), 3449–3450.

MANGER, E. (1996). Modelling and simulation of gas/solid flow in curvilinear coordinates. *Ph.D. thesis*, Telemark Institute of Technology, Norway.

MATHIESEN, V., SOLBERG, T. and HJERTAGER, B. H. (2000a). Prediction of gas/particle flow including a realistic particle size distribution. *Powder Technology* **112**, 34–45.

MATHIESEN, V., SOLBERG, T. and HJERTAGER, B. H. (2000b). An experimental and computational study of multiphase flow behavior in a circulating fluidized bed. *Int. Journal of Multiphase Flow*, **26**(3), 387–419.

MATHIESEN, V. (2000). *Flow Modeling of an Industrial Fluidized Bed Reactor*. AIChE Annual Meeting, Los Angeles, Nov. 12–17, 2000, CFD and its application to fluid-particle systems.

YAKHOT, Y. and ORSZAG, S. A. (1986). Renormalization group analysis of turbulence. Part 1: basis theory. *Journal of Scientific Computing*, **1**(1), 3–51.